Proc. of SPIE Vol. 1170, Fiber Optic Smart Structures and Skins II, ed. E Udd (Feb 1990) Copyright SPIE

Passive and active vibration suppression of large space structures

A. S. Bicos, Y. H. Pak, C. L. Trent, and R. J. Uitto

McDonnell Douglas Space Systems Company
Huntington Beach, California 92647

ABSTRACT

Future spacecraft will have stringent performance requirements that need advanced vibration suppression systems. Examples of these spacecraft are an extended space station, Mission-to-Planet-Earth platforms, and military platforms. Operating conditions for these large space structures (LSSs), e.g., retargeting slew maneuvers and spacecraft docking, can induce unacceptable structural vibrations that take many minutes to naturally dampen out. Increased damping must be added to the structures. This added damping can be a passive mechanism, an active vibration control system, or a combination of passive and active systems. In this investigation, we consider how to satisfy the settling time requirement of a typical LSS. We attempt to determine the amount of vibration suppression or damping necessary to meet the stringent settling time requirement of a typical LSS and then to design, analyze, and experimentally verify an active control system to meet the damping requirement. We also study the effect of passive damping on the active damping system of an LSS to get an idea of what an optimal mix of both passive and active vibration suppression might depend on.

1. INTRODUCTION

Future spacecraft mission requirements necessitate the use of large structures in orbit. Putting these large spacecraft in orbit places stringent requirements on the structure, which include low weight, long life, very good dimensional and dynamic stability, and high damping. Future large space structures (LSSs) include an extended space station, Mission-to-Planet-Earth platforms, and military platforms. Operating conditions for these LSSs, e.g., retargeting slew maneuvers and spacecraft docking, can induce unacceptable structural vibrations that take many minutes to naturally dampen out. Increased damping must be added to the structure. This added damping can be a passive mechanism, an active vibration control system, or a combination of passive and active systems.

Typical truss structures being considered for LSSs exhibit very low modal damping (<0.5%). Owing to the large size (10s to 100s of meters), configuration, and relative low weight, these types of structures will have very low and closely spaced natural frequencies and there can be unwanted interaction of the spacecraft structural response with the control system, i.e., control-structure interaction (CSI). To minimize this interaction (when the controller bandwidth overlaps the structural response bandwidth), the structure's dynamic characteristics must be known as accurately as possible before the spacecraft is put into orbit. Otherwise, a robust, adaptive, or combination controller will be needed because the spacecraft dynamic model that the controller uses, called the plant, has to accurately represent the spacecraft dynamics if the spacecraft is to be precisely controlled. An adaptive or combination controller will need to obtain accurate modal data to modify the plant once on orbit. One way to do this is to use a distributed sensor array. This sensor array could be a network of embedded optical fiber sensors and fiber-optic data

buses. The controller can then use the sensor information to modify the plant and then use the embedded sensor and actuator network to control and suppress the vibration of the structure. This network of embedded fiber-optic sensors also can be used for on-orbit system identification to correct any inaccuracies in the plant and to monitor the health of the structure during its assembly and operational lifetime.

2. PROBLEM AND APPROACH

In this investigation, we consider how to satisfy the settling time requirement of a typical LSS. We attempt to determine the vibration suppression or damping necessary to meet the stringent settling time requirement of a typical LSS and then to design, analyze, and experimentally verify an active control system to meet the damping requirement. We also study the effect of passive damping on the active damping system of an LSS to get an idea of what an optimal mix of both passive and active vibration suppression might depend upon.

3. DAMPING REQUIREMENTS

The existing preliminary design of the Neutral Particle Beam Integrated Space Experiment (NPB-ISE) truss structure was used in this investigation. A detailed NASTRAN model of the NPB platform was developed before the NPB-ISE program was cancelled, therefore, this model was used as the baseline space platform model. The material used in the baseline platform was aluminum. The physical properties of the baseline platform are given in Figure 1.

To determine the damping needed to satisfy space platform mission requirements, we first determined the settling time, defined in the present context as the time between the end of the slew maneuver of the platform and the residual vibration amplitudes becoming less than the allowable deformations. The settling time for a structural mode is a function of the inverse of the product of frequency of that mode and the damping of the structure. The time for the dynamic structural deflections to be reduced to an acceptable level is shortened as the natural frequencies and damping increase. Compared with aluminum, advanced composite materials have up to seven times the specific stiffness, therefore structures using composites have higher frequencies, and up to 10 times the damping.[1,2] Plotted in Figure 2 is the bending vibration amplitude as a function of material specific stiffness for equal geometry beams subjected to the same excitation. Plotted on top of this curve are several points representing typical composite materials and the curve is normalized with respect to the amplitude of an aluminum beam. Figure 2 shows that by using a composite material the amplitude of the response can be significantly reduced without even considering damping. The use of materials with higher specific stiffness to reduce the amplitude of the structural response to acceptable levels may be good enough for some applications but is still far from good enough for the more stringent requirements of a space-based precision optical or weapon system.

The baseline NPB model structural members were redesigned for several composite materials. The members were resized such that the total platform weight remains constant for each design. Then the performance of each was evaluated based on settling time. There are two displacements that settling time depends on, one is the initial displacement at the point of interest due to the residual vibration, and the other is the displacement requirement at the point of interest. The initial displacement depends on the external excitation, in this case the slew maneuver forcing function. Therefore, to obtain an initial displacement typical of a tactical NPB space platform

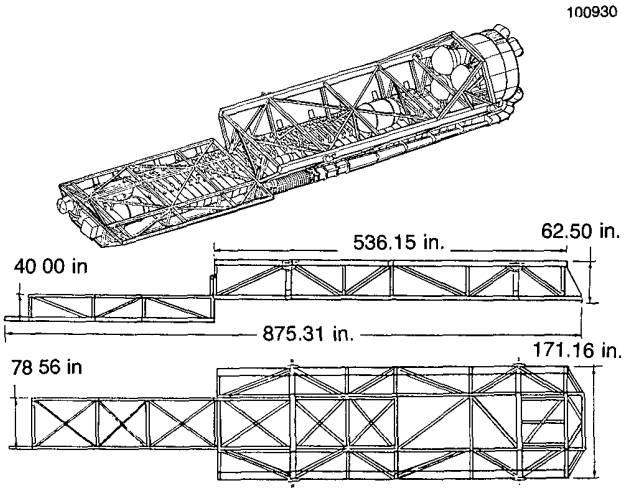

	ISE	Tactical
Length (ft)	76	156
Weight (lb)	41,000	140,000

Fig 1. NPB physical properties.

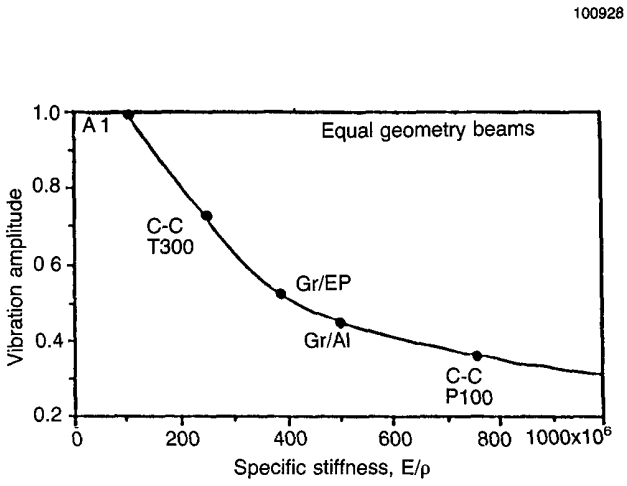

Fig. 2. Amplitude of vibration versus specific stiffness. Amplitudes normalized with respect to aluminum.

during operation a slew maneuver and corresponding thruster forces had to be selected. The typical slew maneuver selected was 10 deg pitch in less than 1 sec. The thrusters were located at the four corners of the main part of the platform (Figure 3a). The thruster forces and firing profile had to be chosen such that the required slew maneuver produced typical initial displacements. The thruster firing profile selected was a bang-bang type tuned to the fundamental frequency of the platform (Figure 3b). The tuning of the thruster firing profile gives reasonable initial displacements and is a first cut at optimizing the thruster firing profile. If the tuning is not done, then unusually large displacements result from the residual vibration (Figure 4). The slew requirement is 10 deg pitch in less than 1 sec, and the resulting magnitude of the thruster forces is about 13,000 lb at each of the four thruster locations. These are large forces, and they induce large stresses in the structure.

The performance of the baseline truss, i.e., the NPB-ISE platform, was determined using the slew maneuver described above. The fundamental frequencies, slew maneuver, thruster force, damping, and settling times are given in Table 1. The settling time for the aluminum baseline platform vibration amplitudes to decrease to below the 0.001-in. requirement at the tracking and pointing system (TPS) location is about 250 sec, which is about 600 times greater than required.

Two advanced composite materials were selected so that a comparison with the performance of the baseline platform could be made. The materials selected were graphite-epoxy (Gr/Ep) and graphite-aluminum (P100-Gr/Al). These materials were chosen because their properties are typical of advanced materials. The baseline truss members were redesigned for each of these materials so that the weight of the structure would remain constant for comparison purposes.

The results for the performance evaluation are given in Table 1, along with the results of the aluminum baseline platform. The settling time is a function of the inverse of the product of the frequency of vibration and the damping at that frequency. Therefore, the larger the frequency and damping, the shorter the settling time. Considering the frequency data alone, the most promising candidate material seems to be the graphite-aluminum. Because of its high specific stiffness, it has the highest fundamental frequencies and thus the shortest settling time if the damping of the materials considered was the same. The damping of the materials, however, is not the same. The

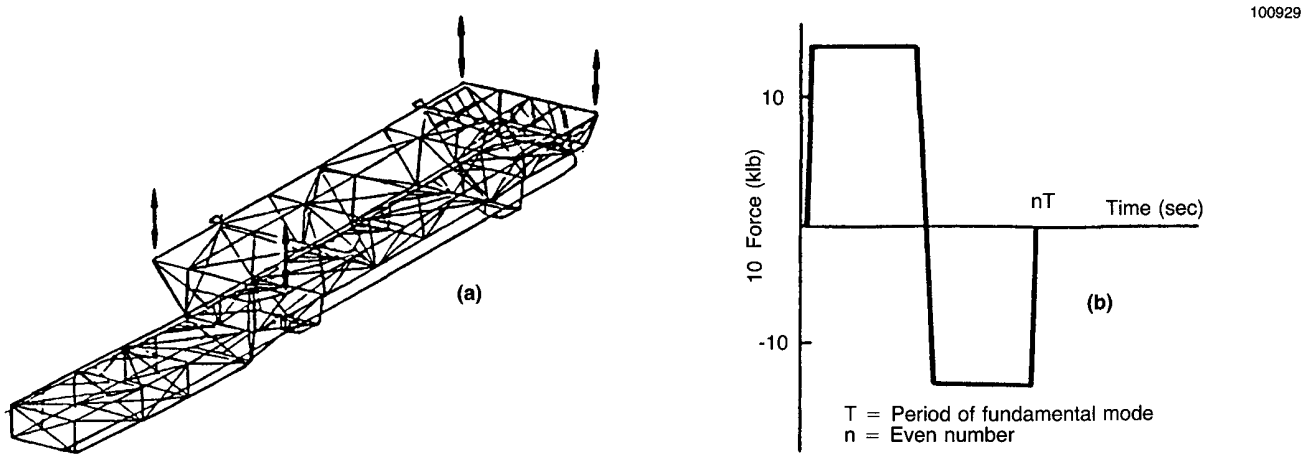

Fig. 3. Thruster locations and directions (a); force profile for each thruster (b).

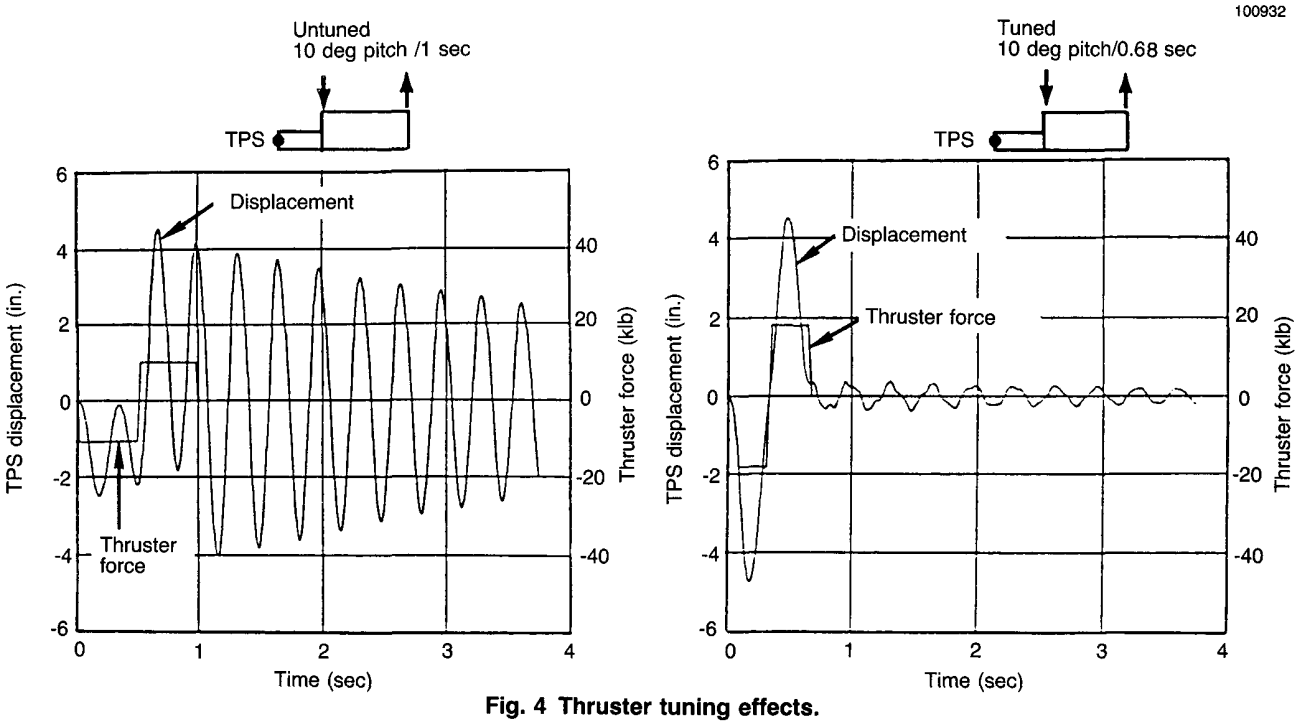

Fig. 4 Thruster tuning effects.

Table 1. Performance Evaluation Based on NPB-ISE NASTRAN Model

Primary Structural Material		Al	Gr/Al	Gr/Ep
Fundamental frequencies (Hz)	Longitudinal bending	2.96	6.15	4 96
	Torsion	4.75	10.04	8 02
	Transverse bending	5 63	11.78	9.50
Tuned 10-deg pitch slew maneuvering time, t_m (sec)		0.676	0 650	0.812
Required thruster force (klb)		13.0	13 5	10 8
Material damping, ζ (%)		0.1	0 1	0 35
Total time: Slew initiation to weapon firing, T_t (sec)		1.1	1.1	1.1
Calculated settling time, T_s (sec)		247	119	43
Required settling time, T_r (sec) $(T_m+T_r \leq T_t)$		0.424	0 450	0.288
Ratio of calculated to required settling time, T_s/T_r		583	264	149

H5189: T1 08/31/89

aluminum and the graphite-aluminum have approximately equal damping factors,[1] while the graphite-epoxy can have many times the damping of aluminum depending on the layup of the composite.[2] Therefore, both the graphite fiber composites are good candidate materials. Assuming typical damping ratios for the materials gives settling times on the order of hundreds of seconds, which is much larger than the required settling times. Therefore, assuming that these are the materials that will be used on SDI-type platform structures, one way to decrease the settling time is to increase the damping in the structure.

If damping is to be added to the structure to decrease the settling time, the question is how much damping is needed in the structure? Using the data in Table 1, the total damping needed by the NPB platform structure can be plotted as a function of the required settling time for the candidate materials (Figure 5). For the graphite-aluminum platform, the total damping needed is about 20 to 30%. The mechanisms inducing the damping have not been specified at this point. This 20 to 30% represents the energy dissipation rate that is required to meet the settling time specification for the NPB platform. The damping mechanisms can be passive, active, or a mix of the two depending on the application and design of the structure.

4. VIBRATION SUPPRESSION

The next step was to design, analyze, and demonstrate a concept to add damping to the structure in the amount determined above. The approach was to (1) simulate the NPB platform bending characteristics using a cantilevered beam with embedded fiber-optic sensors and piezoelectric actuators to demonstrate the necessary control laws; (2) develop a smart strut capable of damping the imposed vibration; and (3) determine the critical locations in the NPB structure for the smart struts to achieve the required level of damping.

4.1 Beam simulator

The pitch and yaw modes of the NPB, as shown in Figure 6, are similar to those for a simple flexible beam. Thus by constructing a simple beam with an appropriate mass distribution, the

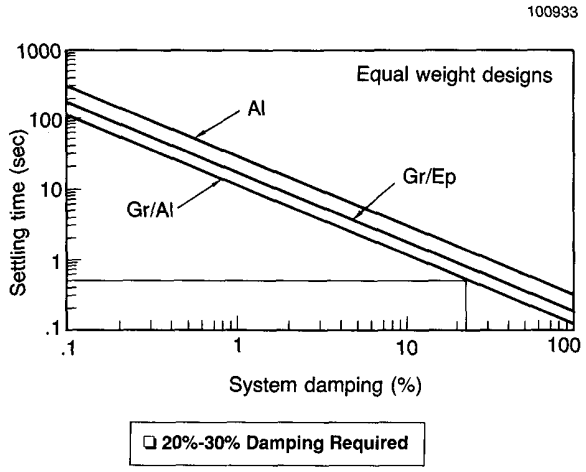

Fig. 5. NPB settling time versus overall system damping.

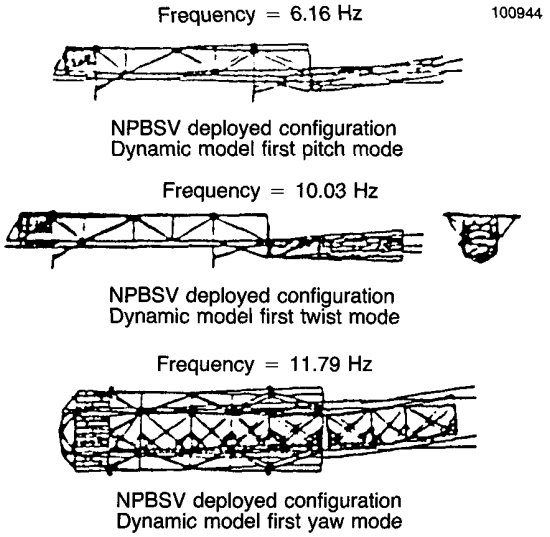

Fig. 6. NPBSV deployed configuration pitch and yaw modes similar to those of a flexible beam.

resulting beam dynamics can be made to approximate the dynamics of the NPB. Once the desired bending frequencies are adequately reproduced on a beam, it can be used as a simple test model to simulate the platform bending characteristics. The control algorithm will then be implemented and verified on the beam, as a proof of concept, to ensure its feasibility to the LSS and to test stability and performance.

In the simulator beam configuration (Figure 7), a total of six piezoelectric-ceramic-actuators (PZAs) and three point-strain fiber-optic sensors are embedded. Each pair of PZAs are embedded at equal distance from the neutral axis of the beam and induce bending moments on the beam cross-section. A point-strain fiber-optic sensor currently being developed is used. Because NPB is structurally stiffer than other types of LSS, and has no moving parts (e.g., an antenna dish, a reflector, or a feed boom), its on-orbit elastic modes are more predictable and large changes in structural behavior are not anticipated. Therefore, for such a structure, actuators can be located at only the most effective locations, i.e., areas of high average strain energy, for the dominant mode or modes (Figure 8). The term "actuator" used in the context of the beam is analogous to a truss member (strut) or a group of struts in an LSS platform. Consequently, if smart struts capable of damping imposed tension or compression forces are selectively placed at those regions of high average strain, overall vehicle damping will occur. Therefore, each PZA in the beam control is actually simulating the role of smart strut(s) in the NPB platform.

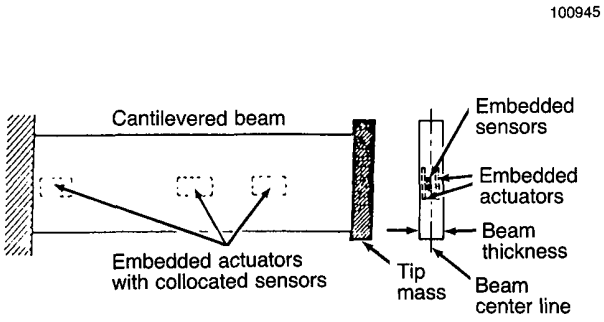

Fig. 7. LSS cantilever beam configuration simulates denseness of NPB resonant frequencies.

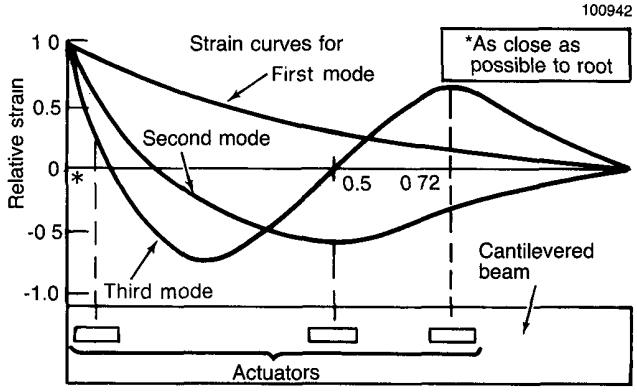

Fig. 8. Most effective actuator locations for cantilevered beam are high strain positions.

4.2 Smart strut design and analysis

A preliminary design of a smart strut with embedded PZAs and an optical-fiber point strain sensor is shown in Figure 9. Dimensions of the strut shown are dimensions of a typical truss member of the NPB. The length and thickness of embedded PZAs are parameters of investigation. For purposes of the analysis, one end of the strut was fixed and a perfect bond between the PZAs and strut was assumed. F_K in the figure represents the imposed linear load on the strut, and dx represents the resulting deformation.

The electromechanical properties of the PZAs used[3] are summarized in Table 2. Because the amount of damping force producible is directly proportional to the dielectric constant (d_{31} term) and stiffness, the PZA with the highest d_{31} value and stiffness is desired.

From the previous NASTRAN analysis, the amount of deformation in a strut at the end of a typical slew was calculated as 0.0115-in. Assuming the same deformation for a smart strut, the amount of force present in the smart strut with PZAs turned off and the maximum damping force

producible with PZAs operating are calculated as the function of PZA length and thickness. They are summarized in Figure 10. The damping force produced by PZAs increases as the length and thickness of PZAs increase. In contrast, the force in the strut decreases at the same time due to the much lower stiffness of the PZA. PZAs, 0.1-in. thick and 50-in. long, can provide a damping force as much as 14% of the imposed force.

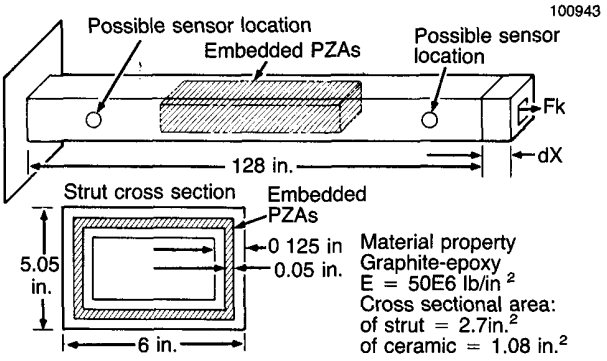

Fig. 9. Preliminary smart struct design uses embedded actuators and point strain sensors.

Table 2. Electromechanical Properties of PZA

Physical properties	Density (x 10^{10} Kg/m 10^{10})	7 45
	Young's Modulus (X = 10^{10} N/m^{10})	6 40
	Curle Temp (C)	1 90
	Mechanical Q, for thin disc	65
Electrical properties	d31 (x 10^{10}-12 M/V)	-262
	r.m s m/V at 25°C	2.0

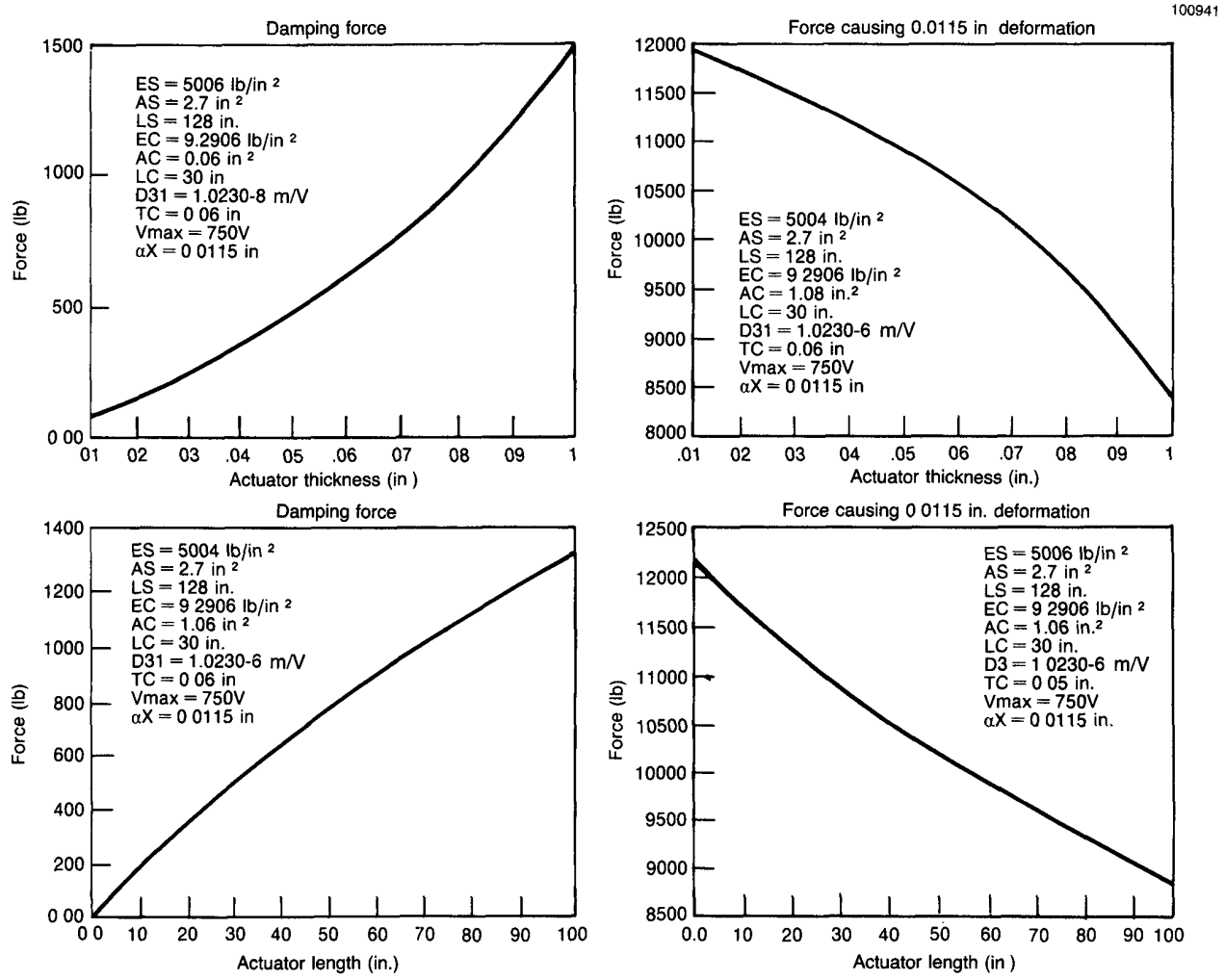

Fig. 10. Damping force increases as thickness and length of PZA increase.

4.3 Beam controller design

The influence of the actuator on the beam can be seen by calculating the generalized force Q acting on the beam.[4]

$$Q = -K_{piezo} \cdot q + Q_V \cdot \lambda$$

where q is the generalized coordinate. The first term reflects the added passive stiffness due to embedding the PZAs, while the second term is a function of the applied input voltage (λ term) and the difference between slope of the beam at the two ends of a PZA (Q_V term). A sensor at each location measures the strain at mid-length of a PZA. A full-order evaluation model written in matrix format in the modal space comprises the first seven modes of the beam.

In designing controllers, three types of control techniques were considered: model error sensitivity suppression (MESS); positivity; and linear quadratic regulator (LQR) reduced order controller. Performance of each type of controller was compared to the LQR full-state feedback (LQSF) controller's. For each controller, all the necessary state information was estimated by either a reduced-order or a full-order observer.

The minimum requirement for each controller was to increase the damping of the first two modes, the most critical modes to NPB performance, to 20% without destabilizing the other modes. The 20% requirement was based on the slew plus settling time requirement imposed on a tactical version of the NPB platform.

The LQSF approach involves designing a full-order (seven modes) observer to estimate the required states and then solving a multiple-input-multiple-output (MIMO) LQR problem to compute the optimal gain matrix K. With a LQSF controller, the desired 20% damping for the first two modes as well as 10% damping for the other modes were achieved (Figure 11). A comparative plot of closed- and open-loop performance is shown in the figure.

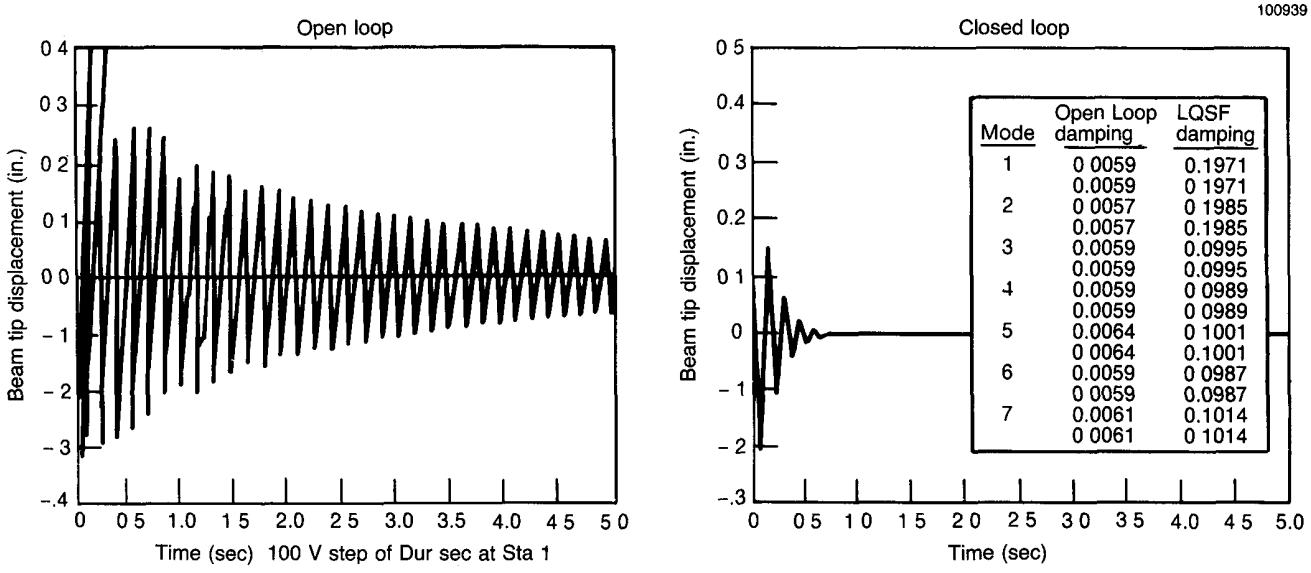

Fig. 11. LQSF controller increases damping by 20% without destabilizing other modes.

The MESS algorithm attempts to drive the control and observation spillover terms to zero without seriously constraining the control authority to controlled states.[5] For the beam, the reduced order controller and observer were designed based on just the first four modes: actively controlling the first two modes while actively suppressing the other two modes. With this four-mode design model, the goal of achieving 20% damping for first and second modes and driving the control and observation spillover to and from the third and fourth modes close to zero was achieved as shown under the first column of Figure 12. Then, the same controller and observer gains are applied to the full-order model to verify its performance against the truth model. The result is shown under the second column of Figure 12. The damping of the first mode is reduced to 7% while the one for the second mode is increased to 23%, and the other modes are undisturbed. The reduction in first mode damping is due to the spillover from those high-frequency modes not included in the initial design model.

To apply the positivity technique to the beam, strain rate sensors were assumed to satisfy the requirement on the plant.[6] Then the plant's positive realness was tested by examining the eigenvalues of $[G(jw)+G^*(jw)]$ as frequency varied, where $G(jw)$ is the square plant matrix. Traces of one of the eigenvalues is shown in Figure 13. This figure, however, indicates that the plant loses its positive realness at the frequency where the eigenvalues cross zero, and therefore violates the positive realness requirement. The exact cause of this phenomenon has not been completely investigated, but it is believed to be due to the unusual dynamics between a point sensor and a non-point (surface) actuator.

The last controller design approach uses internal balancing theory to effectively reduce the order of the system and then, based on that reduced order model (ROM), a reduced order controller (ROC) is designed.

For the beam model, controllability/observability (C/O) gramians for the first four states are the dominant ones, i.e., those states contribute most to the performance objectives. As a result, ROM for this system is just the corresponding 4 x 4 partition of the balanced matrix of the full system. Based on this ROM, a ROC is designed. This ROC design method uses the state aggregation concept[7] for formulating Q and R matrices (state and input weighting matrices) and results in a reduced order standard LQR problem. The resulting ROC is then multiplied by the state aggregation

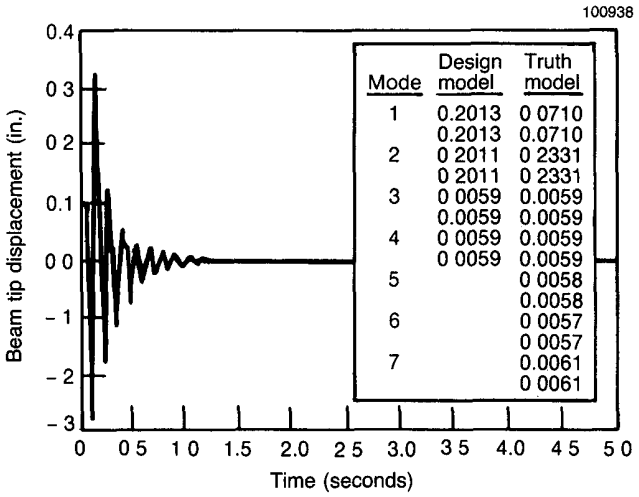

Fig. 12. MESS controller results in reduced damping when verified against truth model.

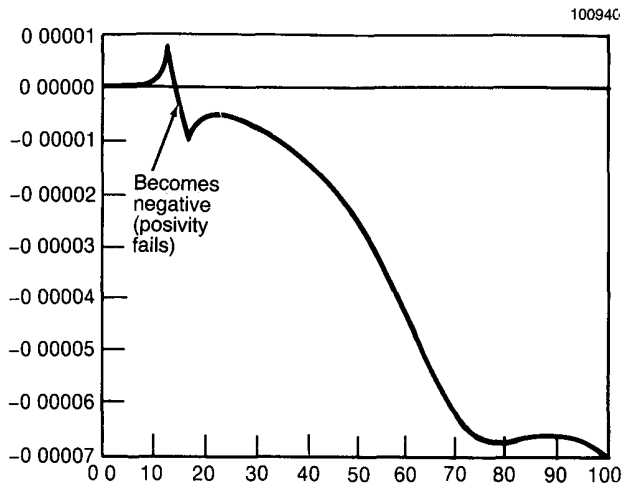

Fig. 13. One of the eigenvalues of [G(jw) + G*(jw)] fails the positive realness.

matrix to form a full-order suboptimal controller. Figure 14 shows the accomplished damping for each mode along with the closed-loop tip deflection. The desired 20% damping was achieved for the first two modes without affecting the higher modes.

In summary, the cantilever beam was used as a simple test model to successfully simulate the dynamic properties of the NPB and to implement and verify the performance of various control designs. The required 20% damping was achieved through LQSF, MESS, and ROC design methods. Positivity design methods would have provided an excellent robustness property against any spillover but owing to the unusual dynamics between a point strain sensor and a surface-covering actuator, the plant failed to meet the positive realness requirement.

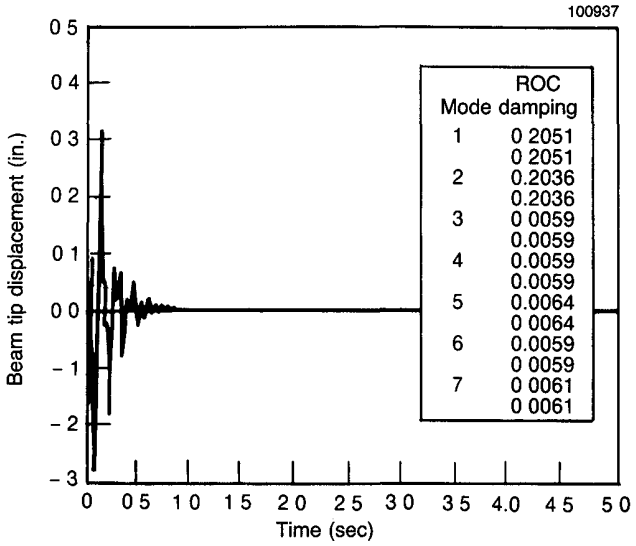

Fig. 14. Reduced order controller achieves 20% damping requirements.

4.4 Identifying optimal locations for smart struts

Although the first-cut optimal slew considerably reduced the residual vibration amplitude of the TPS, it is still far from meeting the requirement (<0.001 in.). Through the NASTRAN analysis of the NPB structure, the strain in each truss member due to the residual vibration resulting from the slew maneuver was determined. Moreover, through PATRAN post-processing of NASTRAN output, the critical truss members were graphically identified as shown in Figure 15. Each truss member is indicated by a different color in the PATRAN output depending on the amplitude of strain energy in that strut. As expected, the truss members located at the intersection of the folding and main section had the highest strain energy, i.e., they are the most critical struts. Consequently, by replacing these critical struts with smart struts capable of actively damping imposed tension and compression deformations the residual vibration can be further reduced.

The function of each smart strut that has replaced a critical strut is to actively increase the damping within each smart strut, which will result in increased overall vehicle damping. In other words, if the dynamics of each strut is represented by the following spring, mass, damper system,

$$Mx'' + Cx' + Kx = F$$

where

M = effective mass of the strut
C = viscoelastic coefficient of the strut
K = spring coefficient of the strut
F = force in the strut

and a prime denotes time differentiation, then, the action of a smart strut is increasing C to $\underline{C}$ where the achievable $\underline{C}$ is governed by the material properties of strut and actuator and the input voltage.

The achievable vehicle damping versus the number of smart struts has been simulated using a NASTRAN model of the NPB. For each set of simulations, a fixed $\underline{C}$ was assigned to each critical strut. Then a series of simulations were performed to determine increase in damping as the number of $\underline{C}$ critical struts is increased. A total of three different $\underline{C}$ values were considered: values that result in 10, 20, or 40% maximum damping. Figure 16 shows the result. The number of $\underline{C}$ critical struts, or smart struts, along the x-axis starts from the most critical strut. It can be concluded from this figure that significant damping can be achieved with a small number of smart struts having high damping.

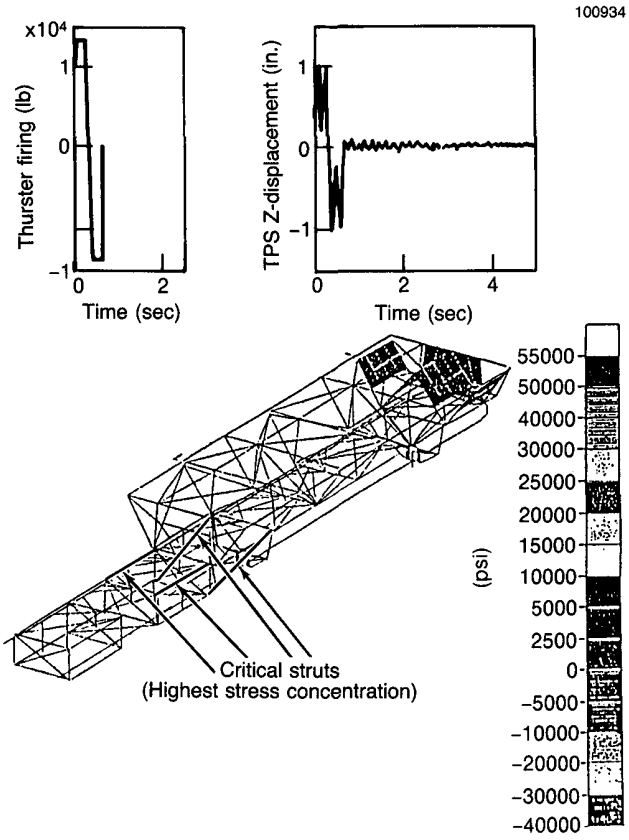

Fig. 15. With PATRAN, critical struts are visibly identified.

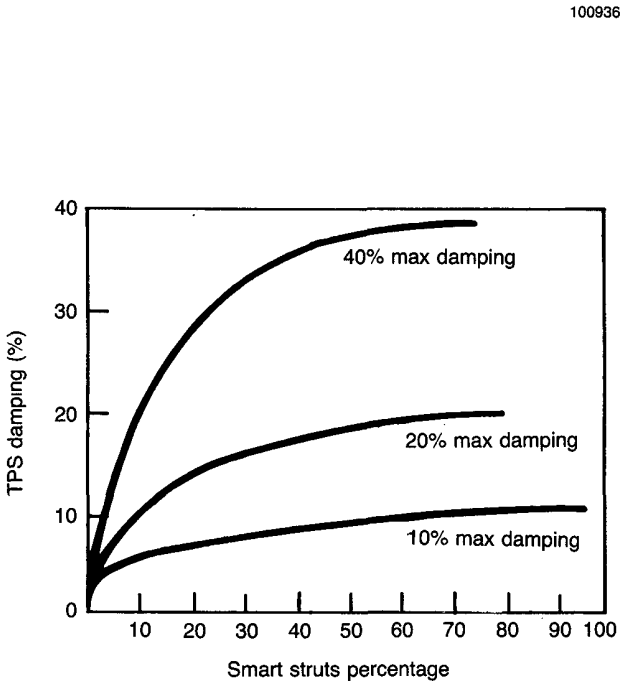

Fig. 16. Twenty percent TPS damping achievable with small number of smart struts.

5. PASSIVE DAMPING EFFECTS ON ACTIVE DAMPING

To determine what the effect of passive damping on the active damping and control of a large space platform is, we used a model of the space station. The excitation to the structure is representative of a space shuttle hard-docking maneuver at the center of the station. We wanted to investigate how a variation in the passive damping affects the required active control system in terms of actuator forces and displacements and structural displacement at the actuator positions.

The actuators selected for this study were proof-mass actuators with the proof-mass component of the actuator weighing 150 lb. There are 81 candidate actuator locations with three directions per location giving a total of 243 candidate actuator positions. A low-authority controller (LAC) and 10 actuator-sensor pairs were selected. The requirement of 15% damping was set. Based on an optimization routine, 10 actuator positions were chosen to give at least 15% active damping to the 10 most critical modes when the passive damping is negligible. The critical modes were chosen based on the amplitude of the rotation at certain payload positions due to the given excitation.

The results of the simulation are presented in Figure 17. The actuator force amplitudes are plotted versus the amount of passive damping. The sum of passive and active damping is always about 15%, which is the requirement set above. As can be seen, the actuator force required drops off with increasing passive damping. The maximum displacement amplitudes of the actuator masses are plotted versus the passive damping. The maximum proof mass displacement decreases with increasing passive damping.

The envisioned design for the space station proof-mass actuators is a 150-lb proof-mass running along a truss member. The space station truss longitudinals and battens are 5 m in length; therefore, if the actuator proof-mass is centered before activation, then the maximum it can displace during a control operation is less than 2.5 m. It can be seen from the plot of actuator

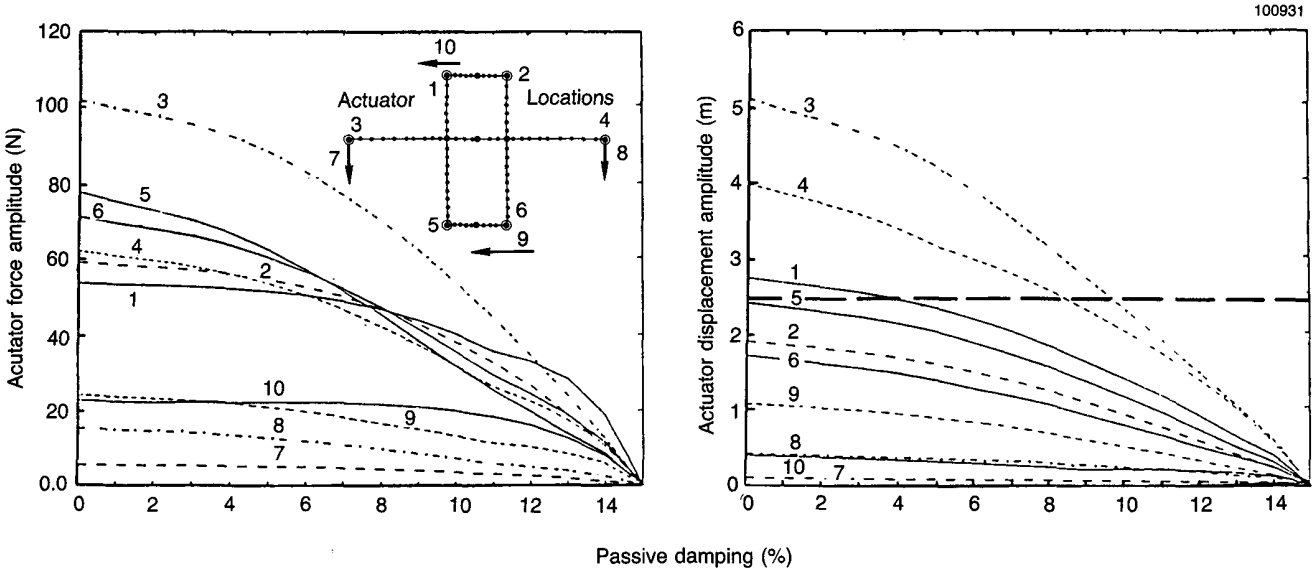

Fig. 17. Effects of increased passive damping.

displacement versus passive damping that if the space station must have at least 15% damping ratio and uses proof-mass actuators, then either the proof-mass of the actuators must increase, the number of sensor-actuator pairs must increase, or the passive damping ratio can be increased to about 11%, which would give a proof-mass displacement of about 2 m.

6. CONCLUSION

Beginning with the construction and operation of the space station, large space platforms to be orbited in the next decade will require varying degrees of damping to perform their missions. In some applications, little or modest levels of damping will be required that can probably be handled with either passive or active methods of energy dissipation. There will be some applications like NPB, however, where much more damping is required, say more than 10% and up to as high as 30%. To achieve these levels of damping performance will require the use of both passive and active damping methods. The active methods being investigated include embedding piezoelectric actuators and fiber-optic sensors using advanced control algorithms. Struts with embedded sensors and actuators can be very effective in damping. The damping force produced is function of its dimension, d_{31} term, stiffness, and input voltage. However, the major concerns are the high input voltage requirement (roughly up to 15 V per 0.001 in.), cost of fabrication, and embedding and curing techniques. As was shown above, the passive and active methods can complement each other, depending on the damping required and the system constraints and characteristics.

7. REFERENCES

1. E. F. Crawley and M. C. van Schoor, Material Damping in Aluminum and Metal-Matrix Composites. *Journal of Composite Materials*, Vol. 21, No. 6, pp. 553-568, 1987.
2. A. S. Bicos, Free Damped Vibration of Composite Plates and Shells. PhD thesis, Stanford University, 1987.
3. EDO Corp., Western Div., Piezo Electric Ceramics Catalog and Application Notes.
4. E. F. Crawley and J. de Luis, Use of Piezoelectric Actuators as Elements of Intelligent Structures. MIT Research Report, Space Systems Laboratory, MIT, Cambridge, MA.
5. J. R. Sesak and P. W. Likens, Model Error Sensitivity Suppression: Quasi-Static Optimal Control for Flexible Structures. IEEE, 1979.
6. M. D. McLaren and G. L. Slater, Robust Multivariable Control of Large Space Structures Using Positivity. *Journal of Guidance*, Vol. 10, No. 4, July-August 1987.
7. S. Hanmann, Model Reduction Using Balanced Representations. Master's thesis, U. of Missouri at Rolla, 1987.